Research Article | Vol. 29, No. 17 / 16 August 2021 / Optics Express 26894
Optics EXPRESS

Theoretical prediction of photophoretic force on a dielectric sphere illuminated by a circularly symmetric high-order Bessel beam: on-axis case

HAIYANG WANG,[1] JIAJIE WANG,[1,3] WENQIANG DONG,[1] YIPING HAN,[1,4] LEONARDO A. AMBROSIO,[2] AND LEI LIU[1]

[1]School of Physics and Optoelectronic Engineering, Xidian University, 710071, Xi'an, China
[2]Department of Electrical and Computer Engineering, São Carlos School of Engineering, University of São Paulo, 400 Trabalhador São-Carlense Ave. 13566-590, São Carlos, SP, Brazil
[3]wangjiajie@xidian.edu.cn
[4]yphan@xidian.edu.cn

Abstract: Compared to the experimental progresses made in the optical trapping of aerosol particles in gaseous media by means of photophoretic forces, the theoretical analysis of photophoretic forces is less developed, the underlying mechanisms being yet not fully understood. In this paper, theoretical derivations of photopheresis of a dielectric sphere in gaseous media illuminated by a circularly symmetric Bessel beam of arbitrary order is presented within the framework of generalized Lorenz-Mie theory. An analytic and closed-form formula for the asymmetry factor, which ultimately determines the sense of direction of photophoretic force, is provided. The influences of particle size, absorptivity of the particle, half-cone angle, beam order of the Bessel beam on the asymmetry factor are explored in detail. The method proposed in this paper can be applied to a wider class of axisymmetric beams carrying nonzero topological charges.

1. Introduction

Optical trapping and manipulation of microparticles in gaseous media by means of photophoretic forces is a promising technique with potential applications in various fields, such as atmospheric chemistry [1,2], particle guiding and sorting [3], optical trap displays for creating three-dimensional images in space [4,5], and others. In recent years, fruitful experimental achievements on the manipulation of microparticles based on photophoretic forces have been reported by using a single focused laser beam [6], two counter-propagating "doughnut" vortex beams [3], by using pulsed or continuous-wave [7], and by other structured laser beams, which makes it possible to manipulate and characterize a wide range of particles of different compositions. More details about optical configurations for trapping and manipulating airborne particles can be found in the review papers by Gong et al. [8,9]. Compare to the fast development in the experimental line, theoretical analysis of photophoretic forces is less developed, the underlying mechanisms are not fully understood.

It has been observed that when illuminated by a beam of light, a microparticle suspended in air performs motion of complex degrees, which depends on the properties of particles (shape, size, material), the parameters of gas media (pressure, composition), and the illumination conditions. A net force, which is called photophoretic force, is exerted on the particles, which results from an uneven momentum transfer between the particle and the gas molecules around the particle surface with temperature gradient. In the case of plane wave illumination, such a force can be either an attractive or a repulsive nature and possess an amplitude orders of magnitude greater than optical forces (gradient and scattering force) for a low-loss particle of a few micrometers.

#433262 https://doi.org/10.1364/OE.433262
Journal © 2021 Received 4 Jun 2021; revised 26 Jul 2021; accepted 27 Jul 2021; published 4 Aug 2021

Optics EXPRESS

The temperature gradient on the surface of the particle is due to the non-uniform absorption of radiant energy within the particle. Thus, the Lorenz-Mie theory was adopted to calculate the source function to formulate radiant absorption distribution within a spherical particle, and then the prediction of photophoretic force. Analytical solutions for photophoretic force can be found, e.g. in Refs. [10,11], where numerical calculations were performed by Pluchino and Antonino [12] for a spherical aerosol particle with radius R much larger than the mean free path ℓ of the surrounding gas molecules (continuous regime) and by Kerker and Cooke [13] for a spherical particle in the free-molecule regime ($R << \ell$). Under certain physical constraints depending upon thermal and hydrodynamic properties of both the particle and the host gaseous medium, closed-form expressions of the photophoretic force were developed for particle in both free molecular and slip-flow regimes by Mackowski [14]. The photophoretic force were expressed in terms of an asymmetry factor J [12], whose calculation depends on the internal field distribution which were derived in infinite-series expression using Lorenz-Mie theory. Recently, Ambrosio [15] extended this method to the case of particles with an arbitrary index of refraction, where negative refractive index and magnetodielectric materials, among others were encompassed.

In the works mentioned above, the photophoretic force was analyzed under an assumption of plane wave illumination. But such a plane wave assumption is not appropriate when a tightly focused laser beam or a structured laser beam, such as vortex beams, is used for illumination. Limited attention has been paid to the prediction of the photophoretic force of a sphere illuminated by a structured beam. Very recently, one of co-authors of this paper, Ambrosio [16] extended the analysis performed by Mackowski for a plane wave illumination to the cases of shaped beam illumination under the framework of the generalized Lorenz-Mie theory (GLMT) [17], which opened a gate for rigorous theoretical investigations on photophoretic forces from structured laser beams of practical interest.

In Ref. [16], expressions of the asymmetry factor for a specific class of on-axis axisymmetric beams of the first kind were presented, where the cases of a fundamental Gaussian beam and a zeroth-order Bessel beam impinging on particles were analyzed. Different from the cases of a fundamental Gaussian beam and a zeroth-order Bessel beam, the Bessel beams of high order are hollow beams, which have several advantages in the optical manipulation of small particles, either by using optical gradient force [18,19] or by using the photophoretic force. In this contribution, the case of on-axis circularly symmetric Bessel beams of an arbitrary order are considered. In this contribution, mathematical derivations for on-axis circularly symmetric Bessel beams of an arbitrary order are considered, which can be applied to the cases of on-axis axisymmetric beams carrying nonzero topological charges.

The rest of this paper is organized as follows. In Section 2, detailed theoretical derivation is presented for photophoretic forces of sphere illuminated by a Bessel beam with arbitrary order. Analytical formula of the asymmetry factor J, which determines the calculation of photophoretic force, is presented in closed-form. Numerical tests and simulation results for the behaviors of asymmetry factor in various conditions are displayed in Section 3. The influences of particle size, refractive index, half-cone angle, beam order of the Bessel beam on the asymmetry factor are explored. Section 4 is a conclusion.

2. Theoretical treatments using GLMT

As illustrated in Fig. 1, a homogeneous dielectric nonvolatile sphere in the gaseous medium is illuminated by a Bessel beam. The conditions for low Reynolds number are assumed to be satisfied. As shown by Mackowski in Eq. (29) and Eq. (39) of Ref. [14], the photophoretic force is directly proportional to the asymmetry factor J, which can be found from the heat source function:

$$J = \frac{3nkx}{2\pi} \int_0^1 t^3 dt \int_0^{2\pi} d\varphi \int_0^{\pi} B(t,\theta,\phi)\cos\theta \sin\theta d\theta. \tag{1}$$

Optics EXPRESS

where $x_p = 2\pi R/\lambda$ and $m_p = n + ik$ are the size parameter and the relative refractive index of the particle, respectively. $B(t, \theta, \phi) = |E(t, \theta, \phi)|^2/E_0^2$ is known as normalized source function [20]. $E(t, \theta, \phi)$ is the electric component of the internal field inside the particle and E_0 its corresponding field strength. The $t = r/R$ is a dimensionless variable.

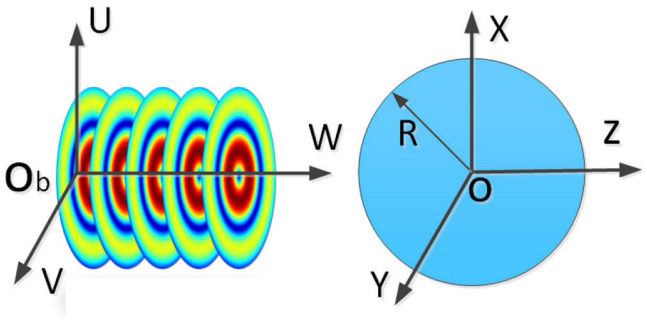

Fig. 1. Illustration of a homogeneous sphere illuminated by an on-axis Bessel beam

As shown in Eq. (1), the asymmetry factor J is a scalar quantity, which involves an integration of the normalized absorbed light intensity over the volume of the particle. Assuming an electromagnetic field propagating along the positive z-axis, positive J or negative J indicates an attractive or repulsive photophoretic force, respectively. Therefore, except when the magnitude of photophoretic forces must be explicitly accounted for, the analysis of photophoretic force can be restricted to an investigation of J which incorporates all information regarding the electromagnetic part of the problem [10].

2.1. GLMT for a Bessel beam scattered by a sphere

Within the framework of GLMT, electric field component of a shaped beam with a time dependence $\exp(-i\omega t)$ can be expanded in terms of vector spherical wave functions (VSWFs) in the coordinate system $Oxyz$ as [17,21]:

$$\mathbf{E}^{inc} = \sum_{n=1}^{\infty}\sum_{m=-n}^{n} E_n[g_{n,TE}^m \mathbf{M}_{mn}^{(1)}(k_0\mathbf{r}) - ig_{n,TM}^m \mathbf{N}_{mn}^{(1)}(k_0\mathbf{r})], \tag{2}$$

where $E_n = i^n E_0(2n + 1)/n(n + 1)$. The k_0 is the wave number in the surrounding medium. The expansion coefficients $g_{n,TE}^m$, $g_{n,TM}^m$ (TE and TM represent transverse electric and transverse magnetic, respectively), known as beam shape coefficients (BSCs), are coefficients encoding the nonuniform illumination of the incident beam. The field amplitude E_0 will be set to unity without any loss of any generality. The VSWFs $\mathbf{M}_{mn}^{(j)}(k\mathbf{r})$ and $\mathbf{N}_{nm}^{(j)}(k\mathbf{r})$ are defined as:

$$\begin{aligned}
\mathbf{M}_{mn}^{(j)}(k\mathbf{r}) =& z_n^{(j)}(kr)\left[\frac{imP_n^{|m|}(\cos\theta)}{\sin\theta}\mathbf{e}_\theta - \frac{dP_n^{|m|}(\cos\theta)}{d\theta}\mathbf{e}_\phi\right]\exp(im\phi) \\
\mathbf{N}_{nm}^{(j)}(k\mathbf{r}) =& \left\{\frac{n(n+1)}{kr} z_n^{(j)}(kr)\, P_n^{|m|}(\cos\theta)\mathbf{e}_r \right. \\
&\left. + \frac{1}{kr}\frac{d[rz_n^{(j)}(kr)]}{dr}\left[\frac{dP_n^{|m|}(\cos\theta)}{d\theta}\mathbf{e}_\theta + \frac{imP_n^{|m|}(\cos\theta)}{\sin\theta}\mathbf{e}_\phi\right]\right\}\exp(im\phi)
\end{aligned} \tag{3}$$

where the $z_n^{(j)}(kr)$ represent the spherical Bessel functions $j_n(kr)$, $y_n(kr)$, $h_n^{(1)}(kr)$ and $h_n^{(2)}(kr)$, respectively, as $j = 1, 2, 3, 4$. The $P_n^{|m|}(\cos\theta)$ is the associated Legendre function.

Optics EXPRESS

Similarly, the components of scattered field and that of the internal field can be expanded in terms of VSWFs as

$$\mathbf{E}^{sca} = \sum_{n=1}^{\infty}\sum_{m=-n}^{n} E_n[ia_{mn}\mathbf{N}_{mn}^{(3)}(k_0\mathbf{r}) - b_{mn}\mathbf{M}_{mn}^{(3)}(k_0\mathbf{r})], \tag{4}$$

$$\mathbf{E}^{int} = \sum_{n=1}^{\infty}\sum_{m=-n}^{n} E_n[c_{mn}\mathbf{M}_{mn}^{(1)}(k_1\mathbf{r}) - id_{mn}\mathbf{N}_{mn}^{(1)}(k_1\mathbf{r})], \tag{5}$$

where k_1 is the wave number inside the particle. It is important to point out that both the scattering coefficients a_{mn}, b_{mn} and the internal field coefficients c_{mn}, d_{mn}, can be expressed as a product of the BSCs $g_{n,TM}^{m}$, $g_{n,TE}^{m}$ and the traditional Mie coefficients as [22–24]:

$$\begin{aligned} a_{mn} &= a_n g_{n,TM}^{m};\ b_{mn} = b_n g_{n,TE}^{m};\\ c_{mn} &= c_n g_{n,TE}^{m};\ d_{mn} = d_n g_{n,TM}^{m};\end{aligned}, \tag{6}$$

where a_n, b_n and c_n, d_n are the scattering and internal field coefficients, respectively, in the classical Lorenz-Mie theory for a plane wave scattered by a sphere. The numerical-ready expressions of a_n, b_n and c_n, d_n can be found in Eqs. (9)–(10) in one of our recent paper [25].

Among various structured beams, there is a great interest in the Bessel beam [26,27], which is mainly due to its special properties, including propagation invariance, self-reconstruction, and the transfer of angular momentum to objects. Prospective applications of Bessel beams can be found in wide range of fields, such as optical communication, biomedicine and optical manipulation. Analytical description of vector circularly symmetric Bessel beams were derived in [28–30]. The circularly symmetric beams have the curious property that neither their longitudinal nor their transverse components of the Poynting vector have any dependence on the azimuth angle. The electric field components of an x-polarized circularly symmetric Bessel beam with its beam center located at an arbitrary point $(x_0,\ y_0,\ z_0)$ are:

$$\begin{aligned} E_x^{(1,0)} &= E_0 g(\alpha_0) e^{ik_z(z-z_0)}\Big\{(1+\cos\alpha_0) i^l e^{il\phi_G} J_l(\sigma_G) - \frac{1}{2}(1-\cos\alpha_0)\\ &\quad\times[i^{l-2}e^{i(l-2)\phi_G}J_{l-2}(\sigma_G) + i^{l+2}e^{i(l+2)\phi_G}J_{l+2}(\sigma_G)]\Big\}\\ E_y^{(1,0)} &= E_0 g(\alpha_0) e^{ik_z(z-z_0)} \frac{1}{2i}(1-\cos\alpha_0)[i^{l-2}e^{i(l-2)\phi_G}J_{l-2}(\sigma_G) - i^{l+2}e^{i(l+2)\phi_G}J_{l+2}(\sigma_G)]\\ E_z^{(1,0)} &= -E_0 g(\alpha_0) e^{ik_z(z-z_0)} \sin\alpha_0[i^{l-1}e^{i(l-1)\phi_G}J_{l-1}(\sigma_G) + i^{l+1}e^{i(l+1)\phi_G}J_{l+1}(\sigma_G)] \end{aligned}, \tag{7}$$

where the superscript (1, 0) which is reminiscent of x-polarization is used, and $\sigma_G = k_t\rho_G$, $\rho_G = [(x-x_0)^2 + (y-y_0)^2]^{1/2}$, $\phi_G = \tan^{-1}[(y-y_0)/(x-x_0)]$. The transverse and longitudinal wave numbers are $k_t = k_0\sin\alpha_0$ and $k_z = k_0\cos\alpha_0$, respectively. The $J_l(\cdot)$ represents a l-order Bessel function of the first kind. The α_0 is the half-cone angle of the Bessel beam. The $g(\alpha_0)$ is a generalization factor. When $g(\alpha_0) = (1+\cos\alpha_0)/4$, the expressions in Eq. (7) reduce to a Davis circularly symmetric Bessel beam. When $g(\alpha_0) = 1/2$, they reduce to those of an angular spectrum representation form of Bessel beam.

A rigorous and efficient approach can be found in Ref. [31] for the calculation of BSCs of a circularly symmetric Bessel beam. Analytical expressions of BSCs in close-form for x-polarized

Optics EXPRESS

circularly symmetric Bessel beam are:

$$\begin{aligned} g^m_{n,TM} &= -g(\alpha_0)(-1)^{\frac{m-|m|}{2}}\frac{(n-m)!}{(n+|m|)!}e^{ikz_0}\{i^{l-m+1}e^{i(l-m+1)\phi_0}J_{l-m+1}(\sigma_0)[\tau^m_n(\cos\alpha_0)+m\pi^m_n(\cos\alpha_0)] \\ &\quad + i^{l-m-1}e^{i(l-m-1)\phi_0}J_{l-m-1}(\sigma_0)[\tau^m_n(\cos\alpha_0)-m\pi^m_n(\cos\alpha_0)]\} \\ g^m_{n,TE} &= ig(\alpha_0)(-1)^{\frac{m-|m|}{2}}\frac{(n-m)!}{(n+|m|)!}e^{ikz_0}\{i^{l-m+1}e^{i(l-m+1)\phi_0}J_{l-m+1}(\sigma_0)[\tau^m_n(\cos\alpha_0)+m\pi^m_n(\cos\alpha_0)] \\ &\quad - i^{l-m-1}e^{i(l-m-1)\phi_0}J_{l-m-1}(\sigma_0)[\tau^m_n(\cos\alpha_0)-m\pi^m_n(\cos\alpha_0)]\}, \end{aligned} \tag{8}$$

where the generalized Legendre functions are introduced

$$\pi^m_n(\cos\alpha_0) = \frac{P^m_n(\cos\alpha_0)}{\sin\alpha_0},\ \tau^m_n(\cos\alpha_0) = \frac{dP^m_n(\cos\alpha_0)}{d\alpha_0}. \tag{9}$$

For an on-axis Bessel beam of l-order, all the BSCs are zero except $m = l \pm 1$, and the BSCs $g^m_{n,TM}$ and $g^m_{n,TE}$ satisfy the relationship [31]:

$$g^{l-1}_{n,TM} = -ig^{l-1}_{n,TE},\ g^{l+1}_{n,TM} = ig^{l+1}_{n,TE}. \tag{10}$$

2.2. Asymmetry factor J for an on-axis high-order Bessel beam scattered by a sphere

In both the slip-flow and the free molecule limit cases, expressions for the photophoretic forces have the same dependency upon radiative absorption, which is embodied in the photophoretic asymmetry factor J. The asymmetry factor J represents a weighted integration of the source function over the particle volume and depends on the intensity of radiative heating, which makes the knowledge of internal field distribution a key issue. In GLMT, the components of the internal electric field in Eq. (5) can be rewritten as:

$$\begin{aligned} E_r &= \frac{-i}{(m_p\rho)^2}\sum_{n=1}^{\infty}\sum_{m=-n}^{n} n(n+1)E_nP^{|m|}_n(\cos\theta)d_{mn}\psi_n(m_p\rho)e^{im\phi} \\ E_\theta &= \frac{1}{m_p\rho}\sum_{n=1}^{\infty}\sum_{m=-n}^{n} E_n\{im\pi^{|m|}_n(\cos\theta)c^{(j)}_{mn}\psi_n(m_p\rho) - i\tau^{|m|}_n(\cos\theta)d^{(j)}_{mn}\psi'_n(m_p\rho)\}e^{im\phi}. \\ E_\phi &= \frac{1}{m_p\rho}\sum_{n=1}^{\infty}\sum_{m=-n}^{n} E_n\{-\tau^{|m|}_n(\cos\theta)c^{(j)}_{mn}\psi_n(m_p\rho) + m\pi^{|m|}_n(\cos\theta)d^{(j)}_{mn}\psi'_n(m_p\rho)\}e^{im\phi} \end{aligned} \tag{11}$$

where $\rho = 2\pi r/\lambda$ is the dimensionless radial coordinate. Considering the relationships of BSCs in Eq. (6) and Eq. (10), Eq. (11) can be rewritten as:

$$\begin{aligned} E_r &= \frac{-i}{(m_p\rho)^2}\sum_{n=1}^{\infty}\sum_{m=l+1,l-1} n(n+1)E_nP^{|m|}_n(\cos\theta)d_ng^m_{n,TM}\psi_n(m_p\rho)e^{im\phi} \\ E_\theta &= \frac{1}{m_p\rho}\sum_{n=1}^{\infty}\sum_{m=l+1,l-1} E_n\{im\pi^{|m|}_n(\cos\theta)c_ng^m_{n,TE}\psi_n(m_p\rho) - i\tau^{|m|}_n(\cos\theta)d_ng^m_{n,TM}\psi'_n(m_p\rho)\}e^{im\phi}. \\ E_\phi &= \frac{1}{m_p\rho}\sum_{n=1}^{\infty}\sum_{m=l+1,l-1} E_n\{-\tau^{|m|}_n(\cos\theta)c_ng^m_{n,TE}\psi_n(m_p\rho) + m\pi^{|m|}_n(\cos\theta)d_ng^m_{n,TM}\psi'_n(m_p\rho)\}e^{im\phi} \end{aligned} \tag{12}$$

Introducing the harmonic function $Y_{n,m} = P^{|m|}_n(\cos\theta)\exp(im\phi), m = 0, \pm1, \pm2 \ldots . \pm n$, the radial field component in Eq. (12) turns to be

$$E_r = \frac{-i}{(m_p\rho)^2}\sum_{n=1}^{\infty}[Y_{n,l+1}(\cos\theta)g^{l+1}_{n,TM} + Y_{n,l-1}(\cos\theta)g^{l-1}_{n,TM}]n(n+1)d_nE_n\psi_n(m_p\rho). \tag{13}$$

Optics EXPRESS

For the radial component of electric field intensity, we have:

$$E_r E_r^* = \frac{1}{|m_p|^4 \rho^4} \sum_{n=1}^{\infty} \sum_{n'=1}^{\infty} n(n+1)n'(n'+1) E_n E_{n'}^* \psi_n \psi_{n'}^* d_n d_{n'}^* \begin{pmatrix} Y_{n,l+1} Y_{n',l+1}^* g_{n,TM}^{l+1} g_{n',TM}^{l+1,*} \\ +Y_{n,l+1} Y_{n',l-1}^* g_{n,TM}^{l+1} g_{n',TM}^{l-1,*} \\ +Y_{n,l-1} Y_{n',l+1}^* g_{n,TM}^{l-1} g_{n',TM}^{l+1,*} \\ +Y_{n,l-1} Y_{n',l-1}^* g_{n,TM}^{l-1} g_{n',TM}^{l-1,*} \end{pmatrix}. \quad (14)$$

Performing an integration over a spherical surface, we have:

$$\int_0^{2\pi} d\varphi \int_0^{\pi} E_r E_r^* \cos\theta \sin\theta d\theta = \frac{1}{|m_p|^4 \rho^4} \sum_{n=1}^{\infty} \sum_{n'=1}^{\infty} n(n+1)n'(n'+1) E_n E_{n'}^* \psi_n \psi_{n'}^* d_n d_{n'}^*$$
$$\times \int_0^{2\pi} d\varphi \int_0^{\pi} \sin\theta \cos\theta d\theta \begin{pmatrix} Y_{n,l+1} Y_{n',l+1}^* g_{n,TM}^{l+1} g_{n',TM}^{l+1,*} \\ +Y_{n,l+1} Y_{n',l-1}^* g_{n,TM}^{l+1} g_{n',TM}^{l-1,*} \\ +Y_{n,l-1} Y_{n',l+1}^* g_{n,TM}^{l-1} g_{n',TM}^{l+1,*} \\ +Y_{n,l-1} Y_{n',l-1}^* g_{n,TM}^{l-1} g_{n',TM}^{l-1,*} \end{pmatrix}. \quad (15)$$

Using the iteration relation of harmonic function (Page 238-239 in Ref. [32]):

$$\cos\theta Y_{n,m} = \frac{1}{N_{n,m}} \left[\sqrt{\frac{(n+|m|)(n-|m|)}{(2n+1)(2n-1)}} N_{n-1,m} Y_{n-1,m} + \sqrt{\frac{(n+|m|+1)(n-|m|+1)}{(2n+1)(2n+3)}} N_{n+1,m} Y_{n+1,m} \right], \quad (16)$$

where $N_{n,m} = \sqrt{\frac{(2n+1)(n-|m|)!}{4\pi(n+|m|)!}}$, $m = 0, \pm 1, \pm 2, \ldots, \pm n$, and then the orthogonal relations:

$$\int_0^{2\pi} d\varphi \int_0^{\pi} \sin\theta d\theta Y_{n,m} Y_{n',m'}^* = \frac{\delta_{m,m'} \delta_{n,n'}}{N_{n,m} N_{n',m'}}$$
$$\int_0^{2\pi} d\varphi \int_0^{\pi} Y_{n,m} Y_{n',m'}^* \cos\theta \sin\theta d\theta = \frac{\delta_{m,m'}}{N_{n+1,m} N_{n,m'}} \sqrt{\frac{(n+|m|+1)(n-|m|+1)}{(2n+1)(2n+3)}} \Lambda_{n,n'}, \quad (17)$$

where

$$\Lambda_{n,n'} = \begin{Bmatrix} 1, |n'-n| = 1, n = \min(n,n') \\ 0, |n'-n| \neq 1 \end{Bmatrix}, \quad (18)$$

In the cases when $m \neq m'$, then:

$$\int_0^{2\pi} d\varphi \int_0^{\pi} \sin\theta d\theta (\cos\theta Y_{n,l+1}) Y_{n',l-1}^* = 0$$
$$\int_0^{2\pi} d\varphi \int_0^{\pi} \sin\theta d\theta (\cos\theta Y_{n,l-1}) Y_{n',l+1}^* = 0, \quad (19)$$

and

$$\int_0^{2\pi} d\varphi \int_0^{\pi} \sin\theta d\theta (\cos\theta Y_{n,l+1}) Y_{n',l+1}^* = \sqrt{\frac{(n+|l+1|+1)(n-|l+1|+1)}{(2n+1)(2n+3)}} \frac{\Lambda_{n,n'}}{N_{n+1,l+1} N_{n,l+1}}$$
$$\int_0^{2\pi} d\varphi \int_0^{\pi} \sin\theta d\theta (\cos\theta Y_{n,l-1}) Y_{n',l-1}^* = \sqrt{\frac{(n+|l-1|+1)(n-|l-1|+1)}{(2n+1)(2n+3)}} \frac{\Lambda_{n,n'}}{N_{n+1,l-1} N_{n,l-1}}, \quad (20)$$

Optics EXPRESS

Then, the integration of radial component of electric field in Eq. (15) simplifies to

$$\int_0^{2\pi} d\varphi \int_0^{\pi} E_r E_r^* \cos\theta \sin\theta d\theta = \frac{1}{|m_p|^4 \rho^4} \sum_{n=1}^{\infty} \sum_{n'=1}^{\infty} n(n+1)n'(n'+1) E_n E_{n'}^* \psi_n \psi_{n'}^* d_n d_{n'}^* \times \int_0^{2\pi} d\varphi \int_0^{\pi} \sin\theta \cos\theta d\theta \begin{pmatrix} Y_{n,l+1} Y_{n',l+1}^* g_{n,TM}^{l+1} g_{n',TM}^{l+1,*} \\ +Y_{n,l-1} Y_{n',l-1}^* g_{n,TM}^{l-1} g_{n',TM}^{l-1,*} \end{pmatrix} . \quad (21)$$

Finally, we have:

$$\int_0^{2\pi} d\varphi \int_0^{\pi} E_r E_r^* \cos\theta \sin\theta d\theta = \frac{-2}{|m_p|^4 \rho^4} \mathrm{Im} \sum_{n=1}^{\infty} \left\{ (2n+1)(2n+3) d_{n+1} d_n^* \psi_{n+1} \psi_n^* \begin{pmatrix} \sqrt{\frac{(n+|l+1|+1)(n-|l+1|+1)}{(2n+1)(2n+3)}} \frac{g_{n+1}^{l+1} g_n^{l+1,*}}{N_{n+1,l+1} N_{n,l+1}} \\ +\sqrt{\frac{(n+|l-1|+1)(n-|l-1|+1)}{(2n+1)(2n+3)}} \frac{g_{n+1}^{l-1} g_n^{l-1,*}}{N_{n+1,l-1} N_{n,l-1}} \end{pmatrix} \right\}, \quad (22)$$

For the transverse components of electric field, considering the relationship of BSCs for an on-axis illumination in Eq. (10), Eq. (12) becomes:

$$E_\theta = \frac{1}{m_p \rho} \sum_{n=1}^{\infty} E_n \left\{ \begin{array}{l} \left[(l+1) \frac{Y_{n,l+1}}{\sin\theta} g_{n,TM}^{l+1} c_n \psi_n(m_p\rho) - i \frac{\partial Y_{n,l+1}}{\partial \theta} d_n g_{n,TM}^{l+1} \psi'_n(m_p\rho) \right] \\ + \left[-(l-1) \frac{Y_{n,l-1}}{\sin\theta} c_n g_{n,TM}^{l-1} \psi_n(m_p\rho) - i \frac{\partial Y_{n,l-1}}{\partial \theta} d_n g_{n,TM}^{l-1} \psi'_n(m_p\rho) \right] \end{array} \right\}$$
$$E_\phi = \frac{1}{m_p \rho} \sum_{n=1}^{\infty} E_n \left\{ \begin{array}{l} \left[i \frac{\partial Y_{n,l+1}}{\partial \theta} c_n g_{n,TM}^{l+1} \psi_n(m_p\rho) + (l+1) \frac{Y_{n,l+1}}{\sin\theta} d_n g_{n,TM}^{l+1} \psi'_n(m_p\rho) \right] \\ + \left[-i \frac{\partial Y_{n,l-1}}{\partial \theta} c_n g_{n,TM}^{l-1} \psi_n(m_p\rho) + (l-1) \frac{Y_{n,l-1}}{\sin\theta} d_n g_{n,TM}^{l-1} \psi'_n(m_p\rho) \right] \end{array} \right\} . \quad (23)$$

The transverse intensity of electric field can be obtained:

$$E_\theta E_\theta^* + E_\phi E_\phi^* = \frac{1}{|m_p|^2 \rho^2} \sum_{n=1}^{\infty} \sum_{n'=1}^{\infty} E_n E_{n'^*} (c_n c_{n'^*} \psi_n \psi_{n'^*} J_1 + i c_n d_{n'^*} \psi_n \psi'_{n'^*} J_2 - i d_n c_{n'^*} \psi'_n \psi_{n'^*} J_3 + d_n d_{n'^*} \psi'_n \psi'_{n'^*} J_4)' \quad (24)$$

where

$$J_q = \begin{pmatrix} (l+1)^2 \frac{Y_{n,l+1}}{\sin\theta} \frac{Y_{n',l+1}^*}{\sin\theta} g_{n,TM}^{l+1} g_{n',TM}^{l+1,*} + (l-1)^2 \frac{Y_{n,l-1}}{\sin\theta} \frac{Y_{n',l-1}^*}{\sin\theta} g_{n,TM}^{l-1} g_{n',TM}^{l-1,*} \\ +(-1)^q (l+1)(l-1) \left[\frac{Y_{n,l+1}}{\sin\theta} \frac{Y_{n',l-1}^*}{\sin\theta} g_{n,TM}^{l+1} g_{n',TM}^{l-1,*} + \frac{Y_{n,l-1}}{\sin\theta} \frac{Y_{n',l+1}^*}{\sin\theta} g_{n,TM}^{l-1} g_{n',TM}^{l+1,*} \right] \\ + \frac{\partial Y_{n,l+1}}{\partial \theta} \frac{\partial Y_{n',l+1}^*}{\partial \theta} g_{n,TM}^{l+1} g_{n',TM}^{l+1,*} + \frac{\partial Y_{n,l-1}}{\partial \theta} \frac{\partial Y_{n',l-1}^*}{\partial \theta} g_{n,TM}^{l-1} g_{n',TM}^{l-1,*} \\ +(-1)^q \left[\frac{\partial Y_{n,l+1}}{\partial \theta} \frac{\partial Y_{n',l-1}^*}{\partial \theta} g_{n,TM}^{l+1} g_{n',TM}^{l-1,*} + \frac{\partial Y_{n,l-1}}{\partial \theta} \frac{\partial Y_{n',l+1}^*}{\partial \theta} g_{n,TM}^{l-1} g_{n',TM}^{l+1,*} \right] \end{pmatrix}, q = 1, 4, \quad (25)$$

$$J_q = \begin{pmatrix} (l+1) \frac{Y_{n,l+1}}{\sin\theta} \frac{\partial Y_{n',l+1}^*}{\partial \theta} g_{n,TM}^{l+1} g_{n',TM}^{l+1,*} - (l-1) \frac{Y_{n,l-1}}{\sin\theta} \frac{\partial Y_{n',l-1}^*}{\partial \theta} g_{n,TM}^{l-1} g_{n',TM}^{l-1,*} \\ +(l+1) \frac{\partial Y_{n,l+1}}{\partial \theta} \frac{Y_{n',l+1}^*}{\sin\theta} g_{n,TM}^{l+1} g_{n',TM}^{l+1,*} - (l-1) \frac{\partial Y_{n,l-1}}{\partial \theta} \frac{Y_{n',l-1}^*}{\sin\theta} g_{n,TM}^{l-1} g_{n',TM}^{l-1,*} \\ +(-1)^q \left[(l+1) \frac{Y_{n,l+1}}{\sin\theta} \frac{\partial Y_{n',l-1}^*}{\partial \theta} g_{n,TM}^{l+1} g_{n',TM}^{l-1,*} + (l-1) \frac{\partial Y_{n,l+1}}{\partial \theta} \frac{Y_{n',l-1}^*}{\sin\theta} g_{n,TM}^{l+1} g_{n',TM}^{l-1,*} \right. \\ \left. -(l+1) \frac{\partial Y_{n,l-1}}{\partial \theta} \frac{Y_{n',l+1}^*}{\sin\theta} g_{n,TM}^{l-1} g_{n',TM}^{l+1,*} - (l-1) \frac{Y_{n,l-1}}{\sin\theta} \frac{\partial Y_{n',l+1}^*}{\partial \theta} g_{n,TM}^{l-1} g_{n',TM}^{l+1,*} \right] \end{pmatrix}, q = 2, 3. \quad (26)$$

Optics EXPRESS

Perform the integration of Eq. (24) over a spherical surface, we have:

$$\int_0^{2\pi} d\varphi \int_0^{\pi} (E_\theta E_\theta^* + E_\varphi E_\varphi^*) \sin\theta \cos\theta d\theta$$
$$= \frac{1}{|m_p|^2 \rho^2} \sum_{n=1}^{\infty} \sum_{n'=1}^{\infty} E_n E_{n'}^* \int_0^{2\pi} d\varphi \int_0^{\pi} \sin\theta \cos\theta d\theta \begin{Bmatrix} c_n c_{n'}^* \psi_n \psi_{n'}^* J_1 \\ +ic_n \psi_n d_{n'}^* \psi_{n'}^{'*} J_2 \\ -id_n \psi_n' c_{n'}^* \psi_{n'}^* J_3 \\ +d_n d_{n'}^* \psi_n' \psi_{n'}^{'*} J_4 \end{Bmatrix}. \quad (27)$$

Using the orthogonal relation of harmonic function (Page 238-239 in Ref. [32]):

$$\int_0^{2\pi} d\varphi \int_0^{\pi} \sin\theta d\theta \times \left(m \frac{Y_{nm}}{\sin\theta} \frac{\partial Y_{n'm'}^*}{\partial \theta} + m' \frac{\partial Y_{nm}}{\partial \theta} \frac{Y^*{}_{n'm'}}{\sin\theta} \right) \cos\theta = \frac{m\delta_{m,m'}\delta_{n,n'}}{N_{n,m} N_{n',m'}}, \quad (28)$$

$$\int_0^{2\pi} d\varphi \int_0^{\pi} \sin\theta d\theta \times \left(mm' \frac{Y_{n,m}}{\sin\theta} \frac{Y_{n',m'}^*}{\sin\theta} + \frac{\partial Y_{n,m}}{\partial \theta} \frac{\partial Y_{n',m'}^*}{\partial \theta} \right) \cos\theta$$
$$= \sqrt{\frac{(n-|m|+1)(n+|m|+1)}{(2n+1)(2n+3)}} n(n+2) \frac{\Lambda_{n,n'}\delta_{m,m'}}{N_{n+1,m} N_{n,m'}}. \quad (29)$$

Thus the integration in Eq. (27) simplifies to

$$\int_0^{2\pi} d\varphi \int_0^{\pi} (E_\theta E_\theta^* + E_\varphi E_\varphi^*) \sin\theta \cos\theta d\theta = \frac{1}{|m_p|^2 \rho^2} \sum_{n=1}^{\infty} \sum_{n'=1}^{\infty} E_n E_{n'}^*$$
$$\times \begin{Bmatrix} (c_n c_{n'}^* \psi_n \psi_{n'}^* + d_n d_{n'}^* \psi_n' \psi_{n'}^{'*}) \begin{pmatrix} \sqrt{\frac{(n-|l+1|+1)(n+|l+1|+1)}{(2n+1)(2n+3)}} n(n+2) \frac{\Lambda_{n,n'}}{N_{n,l+1} N_{n',l+1}} g_{n,TM}^{l+1} g_{n',TM}^{l+1,*} \\ +\sqrt{\frac{(n-|l-1|+1)(n+|l-1|+1)}{(2n+1)(2n+3)}} n(n+2) \frac{\Lambda_{n,n'}}{N_{n,l-1} N_{n',l-1}} g_{n,TM}^{l-1} g_{n',TM}^{l-1,*} \end{pmatrix} \\ +i(c_n \psi_n d_{n'}^* \psi_{n'}^{'*} - d_n \psi_n' c_{n'}^* \psi_{n'}^*) \left[(l+1) g_{n,TM}^{l+1} g_{n',TM}^{l+1,*} \frac{\delta_{n,n'}}{N_{n,l+1} N_{n',l+1}} - (l-1) g_{n,TM}^{l-1} g_{n',TM}^{l-1,*} \frac{\delta_{n,n'}}{N_{n,l-1} N_{n',l-1}} \right] \end{Bmatrix}, \quad (30)$$

Finally, we have:

$$\int_0^{2\pi} d\varphi \int_0^{\pi} (E_\theta E_\theta^* + E_\varphi E_\varphi^*) \sin\theta \cos\theta d\theta = \frac{-2}{|m_p|^2 \rho^2} \times$$
$$\sum_{n=1}^{\infty} \mathrm{Im} \begin{Bmatrix} \frac{(2n+3)(2n+1)}{(n+1)^2} (c_{n+1} c_n^* \psi_{n+1} \psi_n^* + d_{n+1} d_n^* \psi_{n+1}' \psi_n^{'*}) \begin{pmatrix} \sqrt{\frac{(n-|l+1|+1)(n+|l+1|+1)}{(2n+1)(2n+3)}} \frac{g_{n+1,TM}^{l+1} g_{n,TM}^{l+1,*}}{N_{n+1,l+1} N_{n,l+1}} \\ +\sqrt{\frac{(n-|l-1|+1)(n+|l-1|+1)}{(2n+1)(2n+3)}} \frac{g_{n+1,TM}^{l-1} g_{n,TM}^{l-1,*}}{N_{n+1,l-1} N_{n,l-1}} \end{pmatrix} \\ -\frac{(2n+1)^2}{n^2 (n+1)^2} (d_n \psi_n' c_n^* \psi_n^*) \left[(l+1) \frac{g_{n,TM}^{l+1} g_{n,TM}^{l+1,*}}{(N_{n,l+1})^2} - (l-1) \frac{g_{n,TM}^{l-1} g_{n,TM}^{l-1,*}}{(N_{n,l-1})^2} \right] \end{Bmatrix}. \quad (31)$$

Then considering:

$$\psi_{n+1}'(m_p\rho)\psi_{n+1}^{'*}(m_p\rho) = \psi_n \psi_n^{'*} - \frac{(n+1)^2}{|m_p|^2 \rho^2} \psi_{n+1} \psi_n^* + \frac{n+1}{m_p \rho} \psi_{n+1} \psi_{n+1}^*$$
$$\psi_{n+1}(m_p\rho)\psi_n^*(m_p\rho) = \frac{n+1}{m_p \rho} \psi_n \psi_n^* - \psi_n' \psi_n^*, \quad (32)$$

Optics EXPRESS

the integration of total source function becomes:

$$\int_0^{2\pi} d\varphi \int_{-1}^{1} E\cdot E^{*}\cos\theta d\cos\theta = \frac{-2}{|m_p|^2\rho^2}\times$$
$$\mathrm{Im}\sum_{n=1}^{\infty}\left\{\begin{array}{l}\left(\begin{array}{l}\frac{1}{m_p\rho}\frac{(2n+3)(2n+1)}{n+1}(c_{n+1}c_n^{*}|\psi_n|^2+d_{n+1}d_n^{*}|\psi_{n+1}|^2)\left(\begin{array}{l}\sqrt{\frac{(n-|l+1|+1)(n+|l+1|+1)}{(2n+1)(2n+3)}}\frac{g_{n+1,TM}^{l+1}g_{n,TM}^{l+1,*}}{N_{n+1,l+1}N_{n,l+1}}\\+\sqrt{\frac{(n-|l-1|+1)(n+|l-1|+1)}{(2n+1)(2n+3)}}\frac{g_{n+1,TM}^{l-1}g_{n,TM}^{l-1,*}}{N_{n+1,l-1}N_{n,l-1}}\end{array}\right)\end{array}\right)\\-\left\{\begin{array}{l}\frac{(2n+3)(2n+1)}{(n+1)^2}(c_{n+1}c_n^{*}+d_{n+1}d_n^{*})\left(\begin{array}{l}\sqrt{\frac{(n-|l+1|+1)(n+|l+1|+1)}{(2n+1)(2n+3)}}\frac{g_{n+1,TM}^{l+1}g_{n,TM}^{l+1,*}}{N_{n+1,l+1}N_{n,l+1}}\\+\sqrt{\frac{(n-|l-1|+1)(n+|l-1|+1)}{(2n+1)(2n+3)}}\frac{g_{n+1,TM}^{l-1}g_{n,TM}^{l-1,*}}{N_{n+1,l-1}N_{n,l-1}}\end{array}\right)\\+\frac{(2n+1)^2}{n^2(n+1)^2}d_nc_n^{*}\left[(l+1)\frac{g_{n,TM}^{l+1}g_{n,TM}^{l+1,*}}{(N_{n,l+1})^2}-(l-1)\frac{g_{n,TM}^{l-1}g_{n,TM}^{l-1,*}}{(N_{n,l-1})^2}\right]\end{array}\right\}\psi_n'\psi_n^{*}\end{array}\right\},\quad(33)$$

Introducing:

$$\begin{aligned}R_n &= \int_0^x |\psi_n(m_p\rho)|^2dr = \frac{\mathrm{Im}[m_p\psi_{n+1}(m_px)\cdot\psi_n^{*}(m_px)]}{\mathrm{Im}(m_p{}^2)}\\ S_n &= \int_0^x \rho\psi_n{}^{*}(m_p\rho)\psi_n{}'(m_p\rho)dr\\ &= -\frac{i}{2\mathrm{Im}(m_p{}^2)}\left[\begin{array}{c}x(m_p|\psi_n(m_px)|^2+m_p{}^{*}|\psi_{n+1}(m_px)|^2)\\-\left(m_p+2(n+1)\frac{Re(m_p{}^2)}{m_p}\right)R_n+(2n+1)m_p{}^{*}R_{n+1}\end{array}\right]\end{aligned},\quad(34)$$

We then have

$$J=\frac{3nkx}{2\pi x^4}\int_0^x\rho^3d\rho\int_0^{2\pi}d\varphi\int_{-1}^{1}E\cdot E\cos\theta d\cos\theta=\frac{-6nk}{|m_p|^2x^3}\times$$
$$\mathrm{Im}\sum_{n=1}^{\infty}\left\{\begin{array}{l}\left(\begin{array}{l}\frac{(2n+3)(2n+1)}{m_p(n+1)}(c_{n+1}c_n^{*}R_n+d_{n+1}d_n^{*}R_{n+1})\left(\begin{array}{l}\sqrt{\frac{(n-|l+1|+1)(n+|l+1|+1)}{(2n+1)(2n+3)}}\frac{g_{n+1,TM}^{l+1}g_{n,TM}^{l+1,*}}{N_{n+1,l+1}N_{n,l+1}}\\+\sqrt{\frac{(n-|l-1|+1)(n+|l-1|+1)}{(2n+1)(2n+3)}}\frac{g_{n+1,TM}^{l-1}g_{n,TM}^{l-1,*}}{N_{n+1,l-1}N_{n,l-1}}\end{array}\right)\end{array}\right)\\-\left\{\begin{array}{l}\frac{(2n+3)(2n+1)}{(n+1)^2}(c_{n+1}c_n^{*}+d_{n+1}d_n^{*})\left(\begin{array}{l}\sqrt{\frac{(n-|l+1|+1)(n+|l+1|+1)}{(2n+1)(2n+3)}}\frac{g_{n+1,TM}^{l+1}g_{n,TM}^{l+1,*}}{N_{n+1,l+1}N_{n,l+1}}\\+\sqrt{\frac{(n-|l-1|+1)(n+|l-1|+1)}{(2n+1)(2n+3)}}\frac{g_{n+1,TM}^{l-1}g_{n,TM}^{l-1,*}}{N_{n+1,l-1}N_{n,l-1}}\end{array}\right)\\+\frac{(2n+1)^2}{n^2(n+1)^2}d_nc_n^{*}\left[(l+1)\frac{g_{n,TM}^{l+1}g_{n,TM}^{l+1,*}}{(N_{n,l+1})^2}-(l-1)\frac{g_{n,TM}^{l-1}g_{n,TM}^{l-1,*}}{(N_{n,l-1})^2}\right]\end{array}\right\}S_n\end{array}\right\}.\quad(35)$$

Compare to the results presented in Ref. [16], Eq. (35) provides a more general mathematical expression of the asymmetry factor J which is valid for an axisymmetric Bessel beams of an arbitrary order. The Eqs. (34)–(35) are the analytical expressions which can be used directly in the numerical simulations. For more details on the calculation of Eq. (34), please refer to (A1-A6) of Ref. [14].

2.3. Asymmetry factor J for a zeroth-order Bessel beam scattered by a sphere

Specially, for a zeroth-order Bessel beam $l = 0$, according to Eq. (8), the BSCs of an on-axis illumination case satisfies:

$$g_{n,TM}^{1}=g_{n,TM}^{-1}=-ig_{n,TE}^{-1}=ig_{n,TE}^{1}=\frac{g_n}{2},\quad(36)$$

Optics EXPRESS

Equation (35) then reduces to:

$$J = \frac{-6nk}{|m_p|^2 x^3} \mathrm{Im} \sum_{n=1}^{\infty} \left(\begin{array}{l} \frac{n(n+2)}{m_p} g_{n+1} g_n^* (c_{n+1} c_n^* R_n + d_{n+1} d_n^* R_{n+1}) \\ - \left(\frac{n(n+2)}{n+1} g_{n+1} g_n^* (c_{n+1} c_n^* + d_n d_{n+1}^*) + \frac{2n+1}{n(n+1)} g_n g_n^* d_n c_n^* \right) S_n \end{array} \right). \quad (37)$$

which is the same as that given by Ambrosio in Ref. [16] considering a time dependence $\exp(i\omega t)$ was used there. Furthermore, if we set $\alpha = 0°$, the Bessel beam reduces to the case of a plane wave, where $g_n = 1.0$, then Eq. (37) reduces to

$$J = \frac{-6nk}{|m_p|^2 x^3} \mathrm{Im} \sum_{n=1}^{\infty} \left(\begin{array}{l} \frac{n(n+2)}{m_p} (c_{n+1} c_n^* R_n + d_{n+1} d_n^* R_{n+1}) \\ - \left(\frac{n(n+2)}{n+1} (c_{n+1} c_n^* + d_n d_{n+1}^*) + \frac{2n+1}{n(n+1)} d_n c_n^* \right) S_n \end{array} \right). \quad (38)$$

which is the same as that given by Mackowski in Ref. [14] for a plane wave illumination.

3. Numerical results and discussions

Based on the theoretical derivations given in Section 2, a program was written in Fortran 90 to calculate the asymmetry factor J of a sphere illuminated by a circularly symmetric Bessel beam of arbitrary order. To verify the correctness of the theoretical derivation and the code for the asymmetry factor J, the cases of plane wave illumination were verified by setting the half-cone angle of the Bessel beam $\alpha = 0°$ and the order of the beam $l = 0$. The refractive index of the particle are the same as those given in Ref. [14], viz. $m_p = 2 + 1\mathrm{i}$ and $m_p = 1.5 + 0.01\mathrm{i}$ correspond to char particles and fly ash, respectively. The size parameter of the particle $x_p = 2\pi R/\lambda$ ranges from 0.01 to 50. The corresponding curves for $m_p = 1.57 + 0.038\mathrm{i}$ and $m_p = 1.57 + 0.38\mathrm{i}$ were also reproduced and displayed in Fig. 2(a).

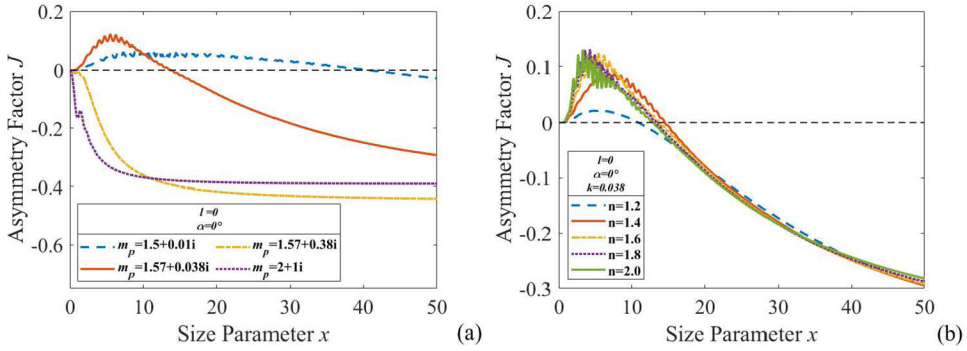

Fig. 2. Variation of J for a zeroth-order Bessel beam with half-cone angle $\alpha = 0°$. (a) reproductions of Fig. 1, Fig. 2 and Fig. 6 in Ref. [14], (b) different real part n of complex refractive index.

The curves in Fig. 2(a) are reproductions of those of Fig. 1, Fig. 2 and Fig. 6 in Ref. [14]. The perfect agreements between our results and those in Ref. [14] are expected since the plane wave illumination is a special case of Bessel beam illumination. This agreement partially indicates the correctness of our theoretical derivations and our home built code.

To explore the influence of real part n of complex refractive index on J, numerical simulations were performed to increase n from 1.2 to 2.0 with a step of 0.1, while the imaginary part is kept constant at k=0.038. Typical results of J spectra are displayed in Fig. 2(b). As we can see from Fig. 2(b), the J's are always positive for particles of small size parameters, which indicates a negative photophoretic force. As n is increased from 1.2 to 1.6, significant changes can be

Optics EXPRESS

observed in the behavior of J for small particles whose size parameters are less than about 20. When n is increased from 1.6 to 2.0, the J spectra are much less sensitive to changes in n than the case when n is increased from 1.2 to 1.6. For particles whose size parameters are larger than 20, the change of n has negligible influence on the J spectra.

To analyze the influence of the half-cone angle on the asymmetric factor J, numerical simulations were performed to increase the half-cone angle of the Bessel beam from zero to 15 degrees with a step of 1 degree. Typical behaviors of the asymmetric factor J with increasing particle size parameter in the case of a zero-order Bessel beam with different half-cone angles are displayed in Fig. 3. Four kinds of particles with different refractive indices (m_p=1.57 + 0.01i, m_p=1.57 + 0.038i, m_p=1.57 + 0.38i, m_p=1.57 + 1.00i) were considered in the simulations.

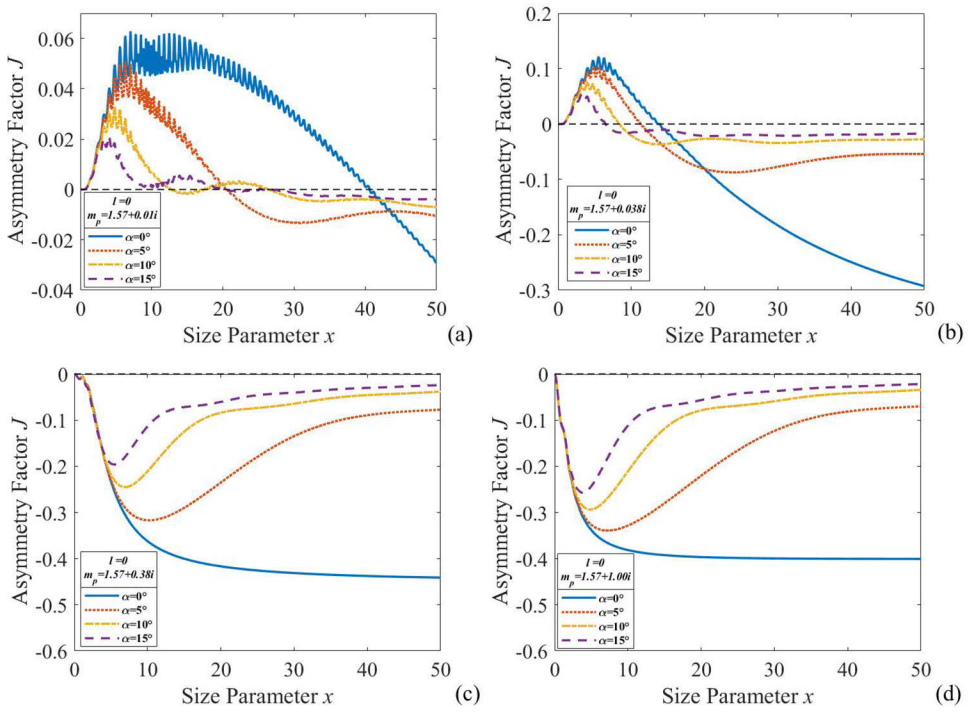

Fig. 3. Variation of J spectra for particles with different refractive indices in the case of a zero-order Bessel beam with different half-cone angles. (a) m_p=1.57 + 0.01i; (b) m_p=1.57 + 0.038i; (c) m_p=1.57 + 0.38i; (d) m_p=1.57 + 1.00i.

As shown in Fig. 3(a) and Fig. 3(b), similar to the case of plane wave illumination, when the absorptivity of the particle is relatively small, the J are always positive for particles of small size parameter, which indicates a negative photophoretic force. With an increase of half-cone angle, the range of size parameters to keep J positive is reduced step by step, which results from the higher focusing of the Bessel beam with larger half-cone angle. If the absorption of the particle is strong, as are the cases in Fig. 3(c) and Fig. 3(d), the values of J are always negative. If, at one hand, the value of J changes significantly with the change of the cone angle for particles whose size parameters are larger than 5, for particles whose size parameters are less than 5, J is essentially insensitive to the change of the cone angle. It is interesting to find that for weak absorption particle, strong oscillation can be found in the J spectra for particles of small size parameter, although this phenomenon is not obvious for large particles. Comparison between the results in Fig. 3(c) with those in Fig. 3(d) leads us to the conclusion that when the absorption of

Optics EXPRESS

the particle is strong enough, the change of imaginary part of complex refractive index k has negligible influence on the J spectra in the cases under study.

To analyze the behaviors of the asymmetric factor J in the cases of Bessel beams of high-orders, numerical simulations were performed for the cases of beam order $l = 1$ and beam order $l = 2$. The variations of the asymmetric factor J with an increase of particle size parameter are displayed in Fig. 4 for Bessel beam with different half-cone angles. The complex refractive index of the absorbing particle is m_p=1.57 + 0.038i. Different from the case of zeroth order, the range of size parameter where the J are positive is very limited. When the size of the particle is small, the absolute value of J is also very small. This is because the Bessel beam of high order is a hollow beam where the intensity at the center of the beam is null.

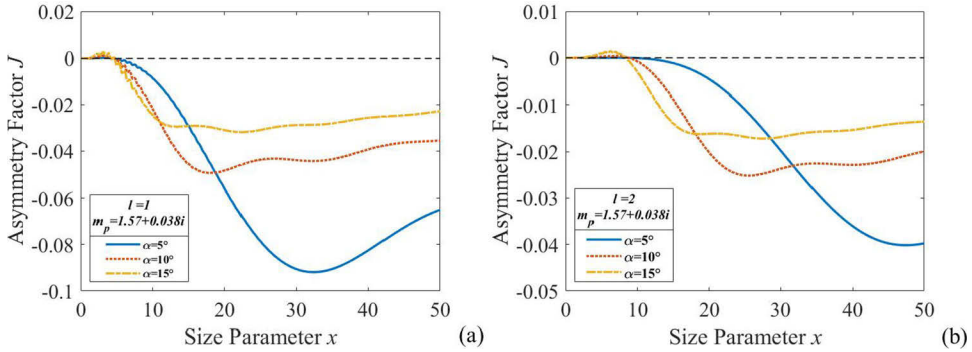

Fig. 4. Variation of J spectra for a high-order Bessel beam with different half-cone angles. The complex refractive index of the particle is m_p=1.57 + 0.038i. (a) $l = 1$;(b) $l = 2$.

To analyze the influence of the imaginary part of the complex refractive index on the behavior of J in the cases of Bessel beam with high order, four kinds of particles with different refractive indices (m_p=1.57 + 0.01i, m_p=1.57 + 0.038i, m_p=1.57 + 0.38i, m_p=1.57 + 1.00i) were considered in the simulations. Curves for the asymmetric factor J as a function of particle size parameter in the case of a Bessel beam illumination with different beam orders are displayed in Fig. 5. The half-cone angle of the Bessel beam is 5 degrees. As shown in Fig. 5, with an increase of absorption, the absolute value of J changes significantly from k=0.01 to k=0.038 and then to k=0.38. Nevertheless, just as in the case of beam order $l = 0$, when absorption within particle is strong enough, the change of imaginary part of complex refractive index k has negligible influence on the J spectra, as is the case when k=0.38 changes to k=1.0.

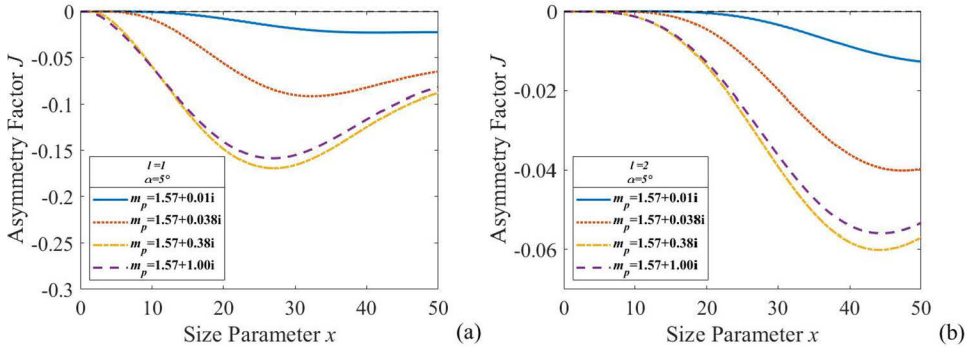

Fig. 5. Variation of J spectra for Bessel beam illumination with different complex refractive indices; The half-cone angle of the Bessel beam is $\alpha = 5°$. (a) $l = 1$;(b) $l = 2$.

Optics EXPRESS

Finally, to explore the influence of the real part of the complex refractive index on J under the illumination of Bessel beam with different orders, simulations are performed by increasing the real part of the complex refractive index from 1.2 to 2.0 with a step of 0.1, for Bessel beam of different orders. Typical results of asymmetric factor J spectra for Bessel beams with $l = 0$, and $l = 1$ are displayed in Fig. 6. The case of $l = 2$ is not displayed since the behavior of J spectra are similar to that of $l = 1$.

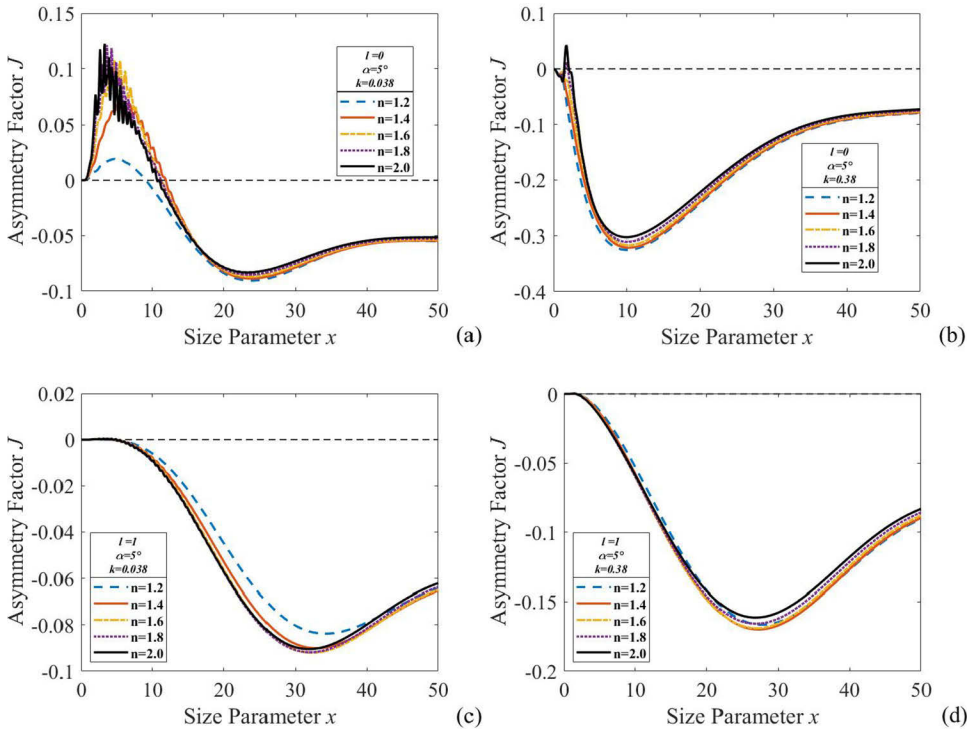

Fig. 6. Comparison of J spectra for Bessel beam illumination with different beam orders and different real parts of the complex refractive index; The half-cone angle of the Bessel beam is $\alpha = 5°$. (a)(c) absorbing particle with m_p=n+0.038i; (b)(d)strong absorbing particle with m_p=n+0.38i;

As shown in Fig. 6, only for particles with weak absorption where k=0.038, the change of real part of the complex refractive index from n=1.2 to n=1.4 has a large influence on the J spectra. For the particle with strong absorption, for instance k=0.38 or with a large value of real part of the complex refractive index, for instance n>1.6, the change of real part of the complex refractive index has very limited influence on the J, compared to the influence of change of the imaginary part.

4. Conclusions

Either motived by applications in atmospheric science and astrophysics, optical trap displays for creating three-dimensional images in space, or in a combination of other techniques, such as imaging, light scattering, Raman spectroscopy, to characterize the physical and chemical properties of the particle itself, the study of photophoretic forces and the optical manipulation of particles in air are now becoming a very attractive topic.

Due to the fact that structured laser beams, such as Bessel beams, have been shown experimentally to have advantages in stably trapping and flexibly manipulation of a particle in air, in this

Optics EXPRESS

paper, a spherical particle illuminated by a circularly symmetric Bessel beam with arbitrary order is analyzed, expressions for J have been derived in closed-form which allows for rapid numerical calculation. The influences of particle size, absorptivity of the particle, half-cone angle, and beam order of the Bessel beam on the asymmetry factor are explored in detail in the numerical simulations. The results shown that the real part of the complex refractive index has very limited influence on the J. Similar to the case of plane wave illumination, J is always positive for particles of small size in the case of zeroth-order Bessel beam, which indicates a negative photophoretic force. If the absorption of the particle is strong, the J are always negative. While the absolute value of the J changes significantly with the change of the half-cone angle, which can be used to adjust the photophoretic force and thus the position of the particle in the beam.

It should be stressed that, although a specific class of on-axis axisymmetric beams of the first kind are considered in Ref. [16] and the derivation in this paper goes beyond to higher order beams with a non-zero net topological charge, the method presented can be extended further to the analysis of photophoretic forces of various regular shaped particles illuminated by arbitrary shaped beams since the interaction of particles in regular shape and arbitrary shaped beam can be rigorously investigated by using the GLMT, which paving the way for theoretical investigations on photophoretic forces from actual laser beams of practical interest. In this paper, we have focused exclusively on the electromagnetic part of the problem, the photophoretic force can be evaluated once other parameters, including the thermodynamic and hydrodynamic conditions, are known. In practical experiments, various forces, including the scattering and gradient forces [18,19] should be addressed to elucidate the trapping mechanism using the structured laser beams, which deserves a further analysis. The Fortran code for producing the results in this paper is available upon request.

Funding. National Natural Science Foundation of China (61501350, 61675159); National Key Laboratory Foundation of China (6142411203109); Conselho Nacional de Desenvolvimento Científico e Tecnológico (307898/2018-0, 426990/2018-8).

Disclosures. The authors declare no conflicts of interest.

Data availability. Data underlying the results presented in this paper are not publicly available at this time but may be obtained from the authors upon reasonable request.

References

1. L. Rkiouak, M. J. Tang, J. C. J. Camp, J. McGregor, I. M. Watson, R. A. Cox, M. Kalberer, A. D. Ward, and F. D. Pope, "Optical trapping and Raman spectroscopy of solid particles," Phys. Chem. Chem. Phys. **16**(23), 11426–11434 (2014).
2. Z. Y. Gong, Y. L. Pan, and C. J. Wang, "Characterization of single airborne particle extinction using the tunable optical trap-cavity ringdown spectroscopy (OT-CRDS) in the UV," Opt. Express **25**(6), 6732–6745 (2017).
3. V. G. Shvedov, A. S. Desyatnikov, A. V. Rode, W. Krolikowski, and Y. S. Kivshar, "Optical guiding of absorbing nanoclusters in air," Opt. Express **17**(7), 5743–5757 (2009).
4. D. E. Smalley, E. Nygaard, K. Squire, J. Van Wagoner, J. Rasmussen, S. Gneiting, K. Qaderi, J. Goodsell, W. Rogers, M. Lindsey, K. Costner, A. Monk, M. Pearson, B. Haymore, and J. Peatross, "A photophoretic-trap volumetric display," Nature **553**(7689), 486–490 (2018).
5. W. Rogers, J. Laney, J. Peatross, and D. Smalley, "Improving photophoretic trap volumetric displays [Invited]," Appl. Opt. **58**(34), G363–G369 (2019).
6. J. Lin and Y. Q. Li, "Optical trapping and rotation of airborne absorbing particles with a single focused laser beam," Appl. Phys. Lett. **104**(10), 101909 (2014).
7. B. Redding, S. C. Hill, D. Alexson, C. J. Wang, and Y. L. Pan, "Photophoretic trapping of airborne particles using ultraviolet illumination," Opt. Express **23**(3), 3630–3639 (2015).
8. Z. Gong, Y. L. Pan, G. Videen, and C. Wang, "Optical trapping and manipulation of single particles in air: Principles, technical details, and applications," J. Quant. Spectrosc. Radiat. Transfer **214**, 94–119 (2018).
9. Z. Y. Gong, Y. L. Pan, and C. J. Wang, "Optical configurations for photophoretic trap of single particles in air," Rev. Sci. Instrum. **87**(10), 103104 (2016).
10. Y. I. Yalamov, V. B. Kutukov, and E. R. Shchukin, "Theory of the photophoretic motion of the large-size volatile aerosol particle," J. Colloid Interface Sci. **57**(3), 564–571 (1976).
11. A. Akhtaruzzaman and S. P. Lin, "Photophoresis of absorbing particles," J. Colloid Interface Sci. **61**(1), 170–182 (1977).
12. A. B. Antonino, "Photophoretic force on particles for low Knudsen number," Appl. Opt. **22**(1), 103–106 (1983).

Optics EXPRESS

13. M. Kerker and D. D. Cooke, "Photophoretic force on aerosol particles in the free-molecule regime," J. Opt. Soc. Am. **72**(9), 1267–1272 (1982).
14. D. W. Mackowski, "Photopheresis of aerosol particles in the free molecular and slip-flow regimes," Int. J. Heat Mass Transfer **32**(5), 843–854 (1989).
15. L. A. Ambrosio, "Photophoresis in the slip-flow and free molecular regimes for arbitrary-index particles," J. Quant. Spectrosc. Radiat. Transfer **255**, 107276 (2020).
16. L. A. Ambrosio, "Longitudinal photophoresis of on-axis axisymmetric beams of the first kind using the generalized Lorenz-Mie theory," Journal of Quantitative Spectroscopy & Radiative Transfer To be published (2021).
17. G. Gouesbet and G. Gréhan, *Generalized Lorenz-Mie Theories Second Edition* (Springer, Berlin, 2017).
18. F. G. Mitri, R. X. Li, L. X. Guo, and C. Y. Ding, "Optical tractor Bessel polarized beams," J. Quant. Spectrosc. Radiat. Transfer **187**, 97–115 (2017).
19. F. G. Mitri, R. X. Li, R. P. Yang, L. X. Guo, and C. Y. Ding, "Optical pulling force on a magneto-dielectric Rayleigh sphere in Bessel tractor polarized beams," J. Quant. Spectrosc. Radiat. Transfer **184**, 360–381 (2016).
20. A. Sarofim, E. Barziv, J. P. Longwell, R. E. Spjut, and W. M. Greene, "Photophoresis of irradiated spheres: absorption centers," J. Opt. Soc. Am. B **2**(6), 998–1004 (1985).
21. G. Gouesbet, "T-matrix formulation and generalized Lorenz-Mie theories in spherical coordinates," Opt. Commun. **283**(4), 517–521 (2010).
22. F. Onofri, G. Grehan, and G. Gouesbet, "Electromagnetic scattering from a multilayered sphere located in an arbitrary beam," Appl. Opt. **34**(30), 7113–7124 (1995).
23. J. J. Wang, T. Wriedt, Y. P. Han, L. Madler, and Y. C. Jiao, "Internal field distribution of a radially inhomogeneous droplet illuminated by an arbitrary shaped beam," J. Quant. Spectrosc. Radiat. Transfer **210**, 19–34 (2018).
24. Z. S. Wu, L. X. Guo, K. F. Ren, G. Gouesbet, and G. Grehan, "Improved algorithm for electromagnetic scattering of plane waves and shaped beams by multilayered spheres," Appl. Opt. **36**(21), 5188–5198 (1997).
25. J. Huang, Y. Zhao, H. Yang, J. Wang, P. Briard, and Y. Han, "Characteristics of photonic jets generated by a dielectric sphere illuminated by a Gaussian beam," Appl. Opt. **59**(21), 6390–6398 (2020).
26. D. McGloin and K. Dholakia, "Bessel beams: diffraction in a new light," Contemp. Phys. **46**(1), 15–28 (2005).
27. D. L. Andrews, *Structured light and its applications : an introduction to phase-structured beams and nanoscale optical forces* (Academic, Amsterdam ; Boston, 2008), pp. xiii, 341 p.
28. J. J. Wang, T. Wriedt, J. A. Lock, and L. Madler, "General description of circularly symmetric Bessel beams of arbitrary order," J. Quant. Spectrosc. Radiat. Transfer **184**, 218–232 (2016).
29. J. J. Wang, T. Wriedt, J. A. Lock, and Y. C. Jiao, "General description of transverse mode Bessel beams and construction of basis Bessel fields," J. Quant. Spectrosc. Radiat. Transfer **195**, 8–17 (2017).
30. F. G. Mitri, R. X. Li, L. X. Guo, and C. Y. Ding, "Resonance scattering of a dielectric sphere illuminated by electromagnetic Bessel non-diffracting (vortex) beams with arbitrary incidence and selective polarizations," Ann. Phys. **363**, 562–563 (2015).
31. J. J. Wang, T. Wriedt, L. Mädler, and Y. P. Han, "Multipole expansion of circularly symmetric Bessel beams of arbitrary order for scattering calculation," Opt. Commun. **387**, 102–109 (2017).
32. Z. X. Wang and D. R. Guo, *Introduction to Special Function*, The Series of Advanced Physics of Peking University (Peking University Press, Beijing, 2000).